Earth and Planetary Science Letters xxx (2010) xxx–xxx

Contents lists available at ScienceDirect

Earth and Planetary Science Letters

journal homepage: www.elsevier.com/locate/epsl

Recent rift-related volcanism in Afar, Ethiopia

David J. Ferguson [a,*], Talfan D. Barnie [b], David M. Pyle [a], Clive Oppenheimer [b], Gezahegn Yirgu [c], Elias Lewi [d], Tesfaye Kidane [c], Simon Carn [e], Ian Hamling [f]

[a] Department of Earth Sciences, University of Oxford, Parks Road, Oxford, OX1 3PR, UK
[b] Department of Geography, University of Cambridge, Downing Place, Cambridge, CB2 3EN, UK
[c] Department of Earth Sciences, University of Addis Ababa, P.O. Box 1176, Addis Ababa, Ethiopia
[d] The Geophysical Observatory, University of Addis Ababa, P.O. Box 1176, Addis Ababa, Ethiopia
[e] Department of Geological and Mining Engineering and Sciences, Michigan Technological University, 1400 Townsend Drive, Houghton, MI 49931, USA
[f] School of Earth and Environment, University of Leeds, Leeds, LS2 9JT, UK

ARTICLE INFO

Article history:
Received 13 October 2009
Received in revised form 4 February 2010
Accepted 5 February 2010
Available online xxxx

Editor: R.W. Carlson

Keywords:
Afar
rift zone volcanism
Ethiopia
remote sensing of volcanoes
basalt

ABSTRACT

Rift zones are the most common magmatic environment on Earth. However opportunities to observe active rifting are rare, and consequently the volcanological characteristics of rift systems are not well understood. An ongoing phase of magmatic rifting along a section of the Red Sea system in Afar, Ethiopia, presents an exceptional opportunity to constrain relationships between volcanism and crustal growth. Here, by integrating analyses of satellite images (i.e. MODIS, OMI, ASTER, and ALI) with field observations, we characterise two recent (August 2007 and June 2009) basaltic fissure eruptions in Afar and evaluate the role and significance of volcanism in the rifting process. Both events were brief (36–72 h) and erupted 4.4–18 $\times 10^6$ m^3 of lava from a fissure system 4–6.5 km in length. Data from the spaceborne Ozone Monitoring Instrument (OMI) suggests total SO_2 emissions for each eruption of 26 ± 5 kt (2007) and 34 ± 7 kt (2009), consistent with complete degassing of the erupted magma volumes. Using geodetic models for the intrusive activity in Afar we estimate the partitioning of magma between intrusive and extrusive components, up to July 2009, to be ~180:1. Comparing the first-order volcanic characteristics and the intrusive–extrusive volume balance for the Afar volcanism with data from the 1975–1984 Krafla rifting cycle (Iceland) suggests that the volcanic flux in Afar will rise significantly over the next few years as the stresses are increasingly relieved by dyking, and subsequent dykes are able to propagate more easily to the surface. As a consequence, basaltic fissure eruptions in this section of the Afar rift will become of increasing large magnitude as the rifting event matures over the next 5–10 yr. Using available models of magmatic rifting we forecast the likely size and location of future eruptions in Afar.

1. Introduction

Rift zones represent the most common magmatic environment on Earth. However, as most magmatic rifts lie inaccessibly on the ocean-floor, and rifting events in terrestrial systems are rare, there have been limited opportunities to characterise rift-related volcanism or the balance between intrusive and extrusive magmatism. Some research has shown that the first-order volcanic characteristics of magmatic rifts, such as flow volumes (Perfit and Chadwick, 1998) and fissure lengths (Sinton et al., 2002), may display consistent variations with spreading rate, implying that the measurement of volcanic eruption parameters can assist in understanding extensional systems. Although observations of ocean-floor rift magmatism at the scale of a single eruption and/or lava flow unit exist (e.g. Chadwick et al., 1995; Embley et al., 2000; Soule et al., 2007), they represent snapshots of otherwise coarse datasets. The ability to document comprehensively a series of eruptions (and associated intrusive activity) in an active magmatic rift is still only practical for subaerial volcanoes. However, subaerial rifting events are infrequent and only one sustained period of activity has been previously observed in the modern instrumental era (i.e. 1975–1984 Krafla rifting phase, Iceland; Bjornsson et al., 1977, 1979; Tryggvason, 1984).

Since September 2005 the Dabbahu–Manda Hararo (DMH) rift zone, a section of the Red Sea system in Afar, Ethiopia (Fig. 1b), has been undergoing a phase of spectacular active rifting, initiated by a large dyking event (<8 m opening along ~60 km of the rift segment accompanied by a small explosive eruption and rhyolite extrusion; Wright et al., 2006; Yirgu et al., 2006; Ayele et al., 2007; Grandin et al., 2009). This was followed by recurring (and ongoing) dyke intrusions

* Corresponding author. Tel.: +44 1865 282119; fax: +44 1865 272072.
E-mail addresses: david.ferguson@earth.ox.ac.uk (D.J. Ferguson), tdb29@cam.ac.uk (T.D. Barnie), david.pyle@earth.ox.ac.uk (D.M. Pyle), co200@cam.ac.uk (C. Oppenheimer), gezahegnyirgu@yahoo.com (G. Yirgu), elias_lewi@yahoo.com (E. Lewi), tesfayek@yahoo.com (T. Kidane), scarn@mtu.edu (S. Carn), i.hamling@see.leeds.ac.uk (I. Hamling).

0012-821X/$ – see front matter © 2010 Elsevier B.V. All rights reserved.
doi:10.1016/j.epsl.2010.02.010

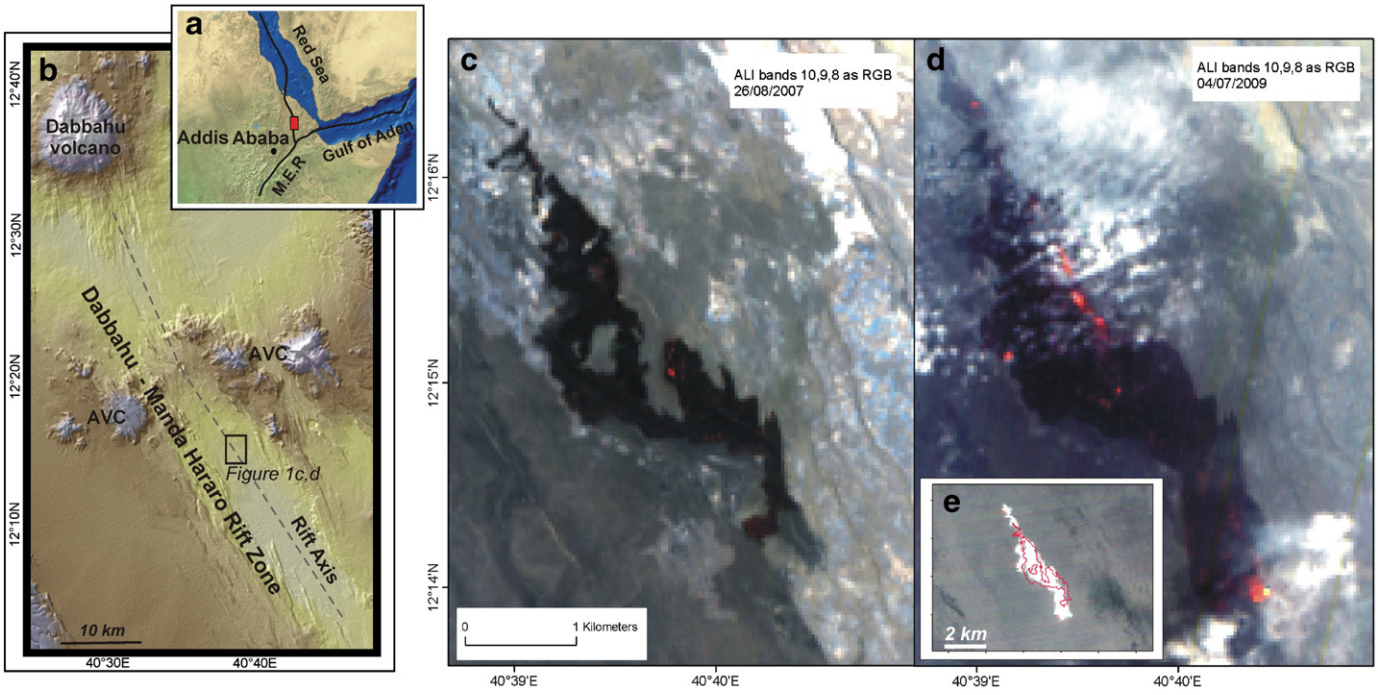

Fig. 1. (a) The Afar triple junction between the Red Sea, Gulf of Aden and Main Ethiopian (MER) rift systems. Box shows the location of the Dabbahu–Manda Hararo rift segment. (b) Shaded ASTER DEM of the Dabbahu–Manda Hararo rift zone. The ~15×60 km segment is entirely floored by basaltic lavas and has two distinct regions erupting more evolved melts; the Dabbahu volcano and the rifted Ado' Ale Volcanic Complex (AVC). (c and d) Daytime Advanced Land Imager (ALI) images of August 2007 and June 2009 fissure eruptions, acquired 12 and 4 days (respectively) following the onset of activity. Both images have the same scale and extent. Bands in the short wave infrared (SWIR) at 2.08–2.35 um, 1.55–1.75 um and 1.2–1.3 um are displayed as RGB respectively. Note the largest scoria cone and SE toe of the 2007 flow and the fissure, SE toe and patches of the 2009 flow were still hot enough at the time of image acquisition to radiate in the far SWIR, and appear red. The August 2007 fissure system was reactivated and extended during the June 2009 eruptions. (e) ASTER night-time temperature image showing area of 2009 flows (2007 eruption outlines in red). (For interpretation of the references to colour in this figure legend, the reader is referred to the web version of this article.)

from a magmatic source located beneath the centre of the rift zone (Keir et al., 2009; Hamling et al., 2009). Thus far, two of the ~13 Afar dyke intrusions have been accompanied by basaltic fissure eruptions. These events present an opportunity to characterise the volcanism associated with an active spreading system, and after ~4 yr of sustained rifting in Afar, we are in a position to analyse the volcanic features of the rift system and draw initial conclusions concerning the partitioning of magma between intrusive and extrusive phases. Here, we present remote sensing and field observations for the two recent rifting-related basaltic eruptions in Afar (August 2007 and June 2009) in order to derive physical parameters for the eruptive systems. These eruptions are comparable in size and duration to some basaltic events reported for oceanic rift systems (i.e. Embley et al., 1999) and therefore may shed light on aspects of magma supply and eruption at oceanic ridges. By comparing the volcanism observed in Afar and at Krafla we evaluate potential temporal trends of magma partitioning between intrusive and extrusive components, and in the magnitude and frequency of basaltic volcanism in Afar.

2. Volcanic–tectonic activity in Afar

The Afar depression in Ethiopia marks the intersection between the Red Sea, Gulf of Aden and East African Rift systems (Fig. 1a). Along the terrestrial portion of the Red Sea system, which runs inland through Eritrea and Ethiopia, extension, seismicity and volcanism are localised at discrete magmatic rift segments (Hayward and Ebinger, 1996). Within these segments, volcanism tends to be bimodal, with extensive basaltic flow fields and axial centres erupting rhyolites (Barberi et al., 1972; Lahitte et al., 2003). Extension across these segments is thought to occur chiefly via the intrusion of dykes into the upper crust (Wright et al., 2006; Rowland et al., 2007; Ebinger et al., 2008).

Magmatic volumes and eruptive frequencies along the Red Sea system in Afar are poorly constrained (e.g. Shaw et al., 1980), as are the relationships between the quantities of magma extruded (as lava flows) as opposed to intruded (as dykes) (e.g. Wadge, 1980; Crisp, 1984; White et al., 2006) the nature of subsurface magma storage/differentiation and eruptive conduit dynamics. Volcanic geomorphology shows considerable variation between rift segments. The DMH rift zone (Fig. 1b), located in the southern part of the Red Sea system, features an axial graben, entirely floored by basaltic lava flows and punctuated along strike by two silicic centres (Rowland et al., 2007). Conversely, the Erta 'Ale range has significant along-axis relief, consisting of volcanic cones and a basaltic caldera that hosts one of the planets few persistently active lava lakes (Oppenheimer and Francis, 1997). These morphological variations suggest that the balance between extensional processes and the volcanic output varies spatially and/or temporally between segments along the rift. Further complexity also arises from the nature of magma differentiation in the crust and the geomorphological consequences of explosive vs. effusive volcanism.

3. Observations of recent basaltic volcanism in Afar

Although more accessible than oceanic rifts, the Afar region is nevertheless a remote and challenging region in which to conduct fieldwork. The eruptions discussed here were first brought to the attention of the international community thanks to timely reports of their associated SO_2 emissions observed by the Ozone Monitoring Instrument (OMI) aboard the EOS-AURA satellite (Smithsonian Institution, 2007, 2009). The location of the SO_2 source was subsequently identified via thermal imagery collected by the MODIS (Moderate Resolution Imaging Spectroradiometer) instrument carried on NASA's Terra and Aqua satellites (e.g. Wright et al., 2004). Rapid field access on both occasions was possible thanks to helicopter

Please cite this article as: Ferguson, D.J., et al., Recent rift-related volcanism in Afar, Ethiopia, Earth Planet. Sci. Lett. (2010), doi:10.1016/j.epsl.2010.02.010

support provided by the Ethiopian Air Force. Both eruptions occurred at the same location; the June 2009 eruption reactivated the August 2007 fissure system and resurfaced the older lavas. Details of the chronology and physical parameters for each eruption are shown in Table 1. Mean effusion rates for both short-lived events (~55–70 $m^3 s^{-1}$) are similar to those reported for fissure eruptions in Iceland (e.g. Harris et al., 2000).

3.1. August 2007 eruption

The August 2007 fissure system was located south of the centre of the DMH segment (Fig. 1b and c). This was the first basaltic eruption since the current rifting phase began (in September 2005) and occurred during the seventh (of thirteen, by end of 2009) dyking event (Hamling et al., 2009). The location of the eruptive fissure coincided with the southern part of the subsurface dyke, as identified through modelling of geodetic data (Hamling et al., 2009) (see Section 5). Thermal data from MODIS indicate that the effusive eruption began on 12 August 2007 and lasted less than 48 h. Visiting the site on 23 August, we observed only residual gas emissions. ASTER (Advanced Spaceborne Thermal Emission and Reflection Radiometer) and Hyperion-ALI satellite imagery of the eruptive system are shown in Fig. 1c and parameters for the eruptive system in Table 1.

3.1.1. Emplacement style

Aspects of the lava flows and their emplacement styles observed during our fieldwork can be recognised by distinctive spectral signatures in the ASTER imagery (~15 m pixel size). This provides the basis for image-based interpretation of the entire flow field and fissure system (Fig. 2a). The fissure system has a total lateral extent of ~4 km, and fed two main lava flows. The northern flow field was sourced from an intermittently active fissure, 2 km in length, whilst a southern fissure around 500 m in length, fed a 1-km-long flow. Constructed along the northern fissure were low (~10 m high) elongate scoria cones that fed pahoehoe flows and sheets that transformed down-flow into channelised aa flows. Activity along the southern fissure constructed three much larger scoria cones (20–30 m in height) and also fed a proximal pahoehoe flow/sheet that became channelled and disrupted down-flow. The tip of the southernmost flow appears to have a pahoehoe texture. Although activity along the southern section appears to have been more explosive (signified by higher scoria cones) and therefore presumably involved more volatile-rich magma, possibly sourced from the head of the intrusion, varying eruptive styles have been observed to occur synchronously along basaltic fissures (e.g. Etna; Spampinato et al., 2008) and the resolution of the MODIS thermal data is insufficient to determine the temporal pattern of activity along the fissure. The total area covered by the new lava flows is 2.2 km^2 and the bulk erupted volume is 4.4–8.8 × 10^6 m^3 (based on flow thickness measured in the field).

3.1.2. SO_2 emissions

SO_2 emissions for both recent eruptions were detected by the Ozone Monitoring Instrument (OMI), a space-based hyperspectral UV/visible spectrometer aboard NASA's Aura satellite (Levelt et al., 2006). Combining SO_2 data from OMI with thermal remote sensing data and field observations allows a more complete evaluation of when the eruptive activity began, diminished and ceased. The SO_2 data presented here are also notable, being one of the few measurements from a basaltic fissure eruption in a transitional/oceanic rift setting; a setting in which the typical degassing behaviour is not well known. Here we use SO_2 total columns derived from the operational OMI SO_2 algorithm (Yang et al., 2007) to calculate SO_2 mass in the volcanic clouds. The first OMI acquisition following the onset of the eruption was on 13 August at 10:15 UTC which detected an SO_2 cloud, emanating from the DMH region over Ethiopia and Sudan. A further acquisition on 14 August showed these emissions to be continuing, however the thermal signal in the MODIS data had significantly decreased, indicating that the effusion of lava had probably ceased. Estimates of the SO_2 mass from the OMI data are very sensitive to the altitude of the SO_2 cloud. A forward trajectory model for the plume (using the HYbrid Single-Particle Lagrangian Integrated Trajectory model, HYSPLIT; Draxler and Rolph, 2003) suggests an altitude of 3–5 km. Downwind lofting of the cloud suggested by this model is caused by the large increase in elevation over the Ethiopian highlands (max elevation ~4.5 km). Assuming a maximum altitude of 5 km gives an approximate SO_2 mass of 26 ± 5 kt. No data are currently available on the un-degassed volatile contents of the DHM magmas, however peak sulfur concentrations from olivine-hosted melt inclusions from young basalts in the nearby Asal rift reach ~0.12 wt.% (Clocchiatti et al., 1980). Our analysis of glassy scoria from this eruption (Table 2, samples A2–3) show that the sulfur content of the erupted and degassed magma is 0.023–0.038 wt.% (Table 2). If we assume a typical sulfur loss of 0.09 wt.% during ascent and eruption, the observed emission of 26 kt (26 × 10^6 kg) of SO_2 would require around 5.5 × 10^6 m^3 of magma. The bulk erupted volume estimated from field and RS observations of 4.4–8.8 × 10^6 m^3 is in good agreement with this and is sufficient to account for all of the observed SO_2 released without needing to invoke volatile loss from un-erupted melt (i.e. no "excess" sulfur).

3.2. June 2009 eruption

Following the August 2007 fissure eruption, the central and southern sections of the DMH rift were re-intruded by five further dykes with an average return time of ~4 months. The sixth dyke intrusion since August 2007 (and 13th since September 2005) coincided with a second extrusive event in June 2009. During this event, the August 2007 eruptive fissure was reactivated, the new eruption products almost entirely covering the earlier flows (Fig. 1d). The first thermal alerts from MODIS were recorded on 28 June at 23:20 UTC. These had subsided by 2 July 2009. An Advanced Land Imager (ALI) image acquired on 4 July 2009, the same day as a field visit, clearly shows the newly emplaced flows and the residual heat along the main fissure and across the lava flows. This was also imaged from a helicopter using an infrared camera (a FLIR Thermacam) and a maximum temperature of 375 °C recorded at the surface of the fissure (Fig. 2c). On site, we observed newly constructed scoria cones, ~50 m in height, from which moderate gas emissions were still occurring (Fig. 2b and c). New fissures, with surface openings of ≤0.5 m, were

Table 1
Summary of parameters for the August2007 and June 2009 Afar eruptions.

Eruption date	Duration of main effusive phase[a]	Total fissure length (km)	Area (km^2)	Bulk volume (10^6 m^3)	Intrusive: Extrusive	Mean effusion rate ($m^3 s^{-1}$)	Bulk SO_2 flux[b] (kt)
August 2007	36–48 h	4	2.2	4.4–8.8	~10:1	55	26 ± 5
June 2009	48–60 h	6.5	4.5	13–18	~5:1	70	34 ± 7

[a] Estimated from MODIS thermal data.
[b] Measured by the Ozone Measuring Instrument (OMI).

Please cite this article as: Ferguson, D.J., et al., Recent rift-related volcanism in Afar, Ethiopia, Earth Planet. Sci. Lett. (2010), doi:10.1016/j.epsl.2010.02.010

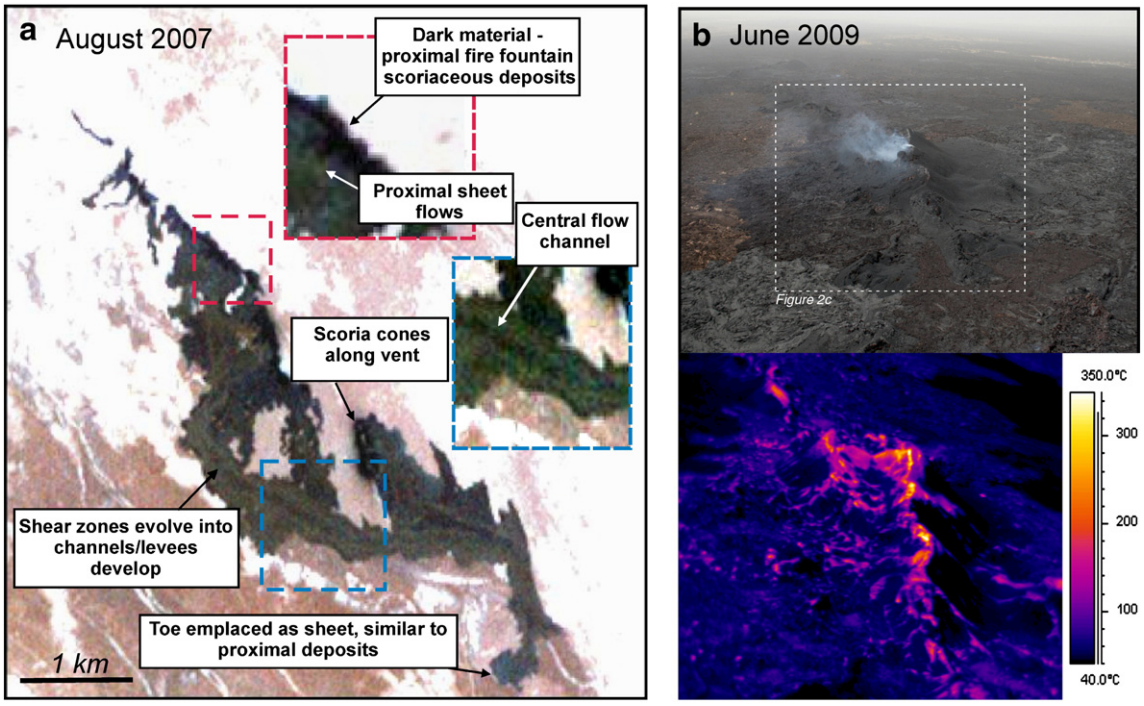

Fig. 2. (a) Interpreted visible-near infrared (VNIR) ASTER image of August 2007 eruption products. Image resolution is 15 m. Image histogram for each RGB channel has been stretched to highlight spectral variation over very low reflectance fresh basalts. Eruption products identified from oblique aerial photographs and ground inspection can be recognised in the ASTER image and different emplacement styles identified. Relatively unfractured pahoehoe surfaces appear blue, fractured aa surfaces appear grey-brown, scoria dark blue–black, previous aa lava flows pale brown, old flows and sediment white. (b)Visual and (c) thermal images of the June 2009 eruptive vent taken from a helicopter on 4 July 2009 (eruption began 29 June 2009). Scoria appears smooth and dark grey, pahoehoe light–medium grey, heavily fractured aa material brown. Temperature image acquired with a FLIRThermacam. Highest recorded temperature in this image is 375 °C. (For interpretation of the references to colour in this figure legend, the reader is referred to the web version of this article.)

also observed around the vicinity of the eruptive vents, as were fresh looking fault surfaces with vertical throws of ≤1.5 m.

3.2.1. Emplacement style and physical parameters

As with the August 2007 eruption, the proximal lava flows were emplaced as pahoehoe type flows that evolved into aa flows away from the vent. Channelisation of the flows was less distinct than in the 2007 eruption. Eruptive activity was concentrated in the northern section of the fissure, the site of the most intense degassing and thermal signature in the ALI image (Figs. 1d and 2b, c). The eruption reactivated the entire length of the 2007 fissure and extended the system by ~500 m to the south and 1 km to the north. The active fissure was more continuous than observed for the 2007 eruption, and had a total length of 5.2 km. Although largely overlying the previous lava flows, the areal extent of the new eruption products can be estimated from ASTER night-time thermal data (Fig. 1e). The new lava flows and proximal scoria deposits cover an area of 4.5 km^2 with a total erupted bulk volume of 13.5–18 × 10^6 m^3 (using field observation of flow thickness). Physical parameters are summarised in Table 1.

3.2.2. SO_2 emissions

The first SO_2 detection by OMI was on 29 June at 10:23 UTC (Fig. 3). Infrared satellite instruments that have poor sensitivity to the lower troposphere (e.g., AIRS and IASI) detected no SO_2 during the eruption, from which we infer a plume altitude of <5 km. On this occasion radiosonde data is available from a launch site in Saudi Arabia (18.2°N, 42.7°E), which indicates a wind speed at <5 km of 10.3 m s^{-1} from the NE. Above this altitude a strong shear wind was present, which is also consistent with a lower tropospheric plume. HYSPLIT modelling again suggests an altitude of 3–5 km. In the first OMI detection, shown in Fig. 3, the plume was drifting ~SW and contained 15–36 kt of SO_2 (depending on altitude). In this image a concentrated pulse of SO_2 is visible in the centre of the cloud, around 384 km downwind of the source, presumably relating to the most vigorous stage of the eruption. With a wind speed of 10.3 m s^{-1} this distance suggests around ~10 h of transport. This is very close to the time of the first MODIS thermal alerts and presumably the onset of lava effusion. The next OMI acquisition on 30 June at 11:06 UTC also detected tropospheric SO_2 over western Ethiopia and Sudan, however due to a data gap the measurements did not cover the plume in the area around the eruption site. Assuming an altitude of 5 km gives a total SO_2 mass of 34 ± 7 kt. Due to the data gap in the second acquisition this is likely a minimum estimate. Using our inferred value for sulfur loss during decompression, (see Section 3.1.2) the observed emissions of 34 × 10^6 kg of SO_2 would require degassing from ~7 × 10^6 m^3 of magma. Considering the gap in the OMI data it seems reasonable to assume that all the emitted SO_2 can be accounted for by the erupted bulk volume of 13.5–18 × 10^6 m^3.

4. Geochemistry

Samples for geochemical analysis were collected during each field visit, and the full details of this ongoing work will be published in due course. We present a summary of whole rock major element compositions, Ni contents and normative mineralogy for samples from each eruption in Table 2. As the 2007 eruption site was visited for a second time around 6 months after the eruption it was possible to collect both crystalline samples (sample A1) and also glassy scoria from around the fissure (samples A2–3). The 2009 eruption however was only visited immediately following the event and it was only possible to collect crystalline samples from the lava flow fronts at that time (samples B1–4). Both eruptions produced hypersthene-normative basaltic lavas, with SiO_2 contents of 48–49 wt.% and total alkali contents of 3.7–3.8 wt.%. As with older basalts erupted near the Dabbahu volcano (Barberi et al., 1975) and further south along the

Please cite this article as: Ferguson, D.J., et al., Recent rift-related volcanism in Afar, Ethiopia, Earth Planet. Sci. Lett. (2010), doi:10.1016/j.epsl.2010.02.010

Table 2
Whole rock major element compositions (wt.% oxide), normative mineralogy and Mg-number for basaltic lavas erupted in Afar August 2007 and June 2009.

Eruption date	August 2007			June 2009				
Sample	A1[a]	A2[b]	A3[b]	B1[a]	B2[a]	B3[a]	B4[a]	Error (1σ)
Location	12° 15′ 47.5 40° 39′ 07.5	12° 15′ 54.4 40° 39′ 13	12° 15′ 53.6 40° 39′ 14.1	12° 15′ 21 40° 39′ 05.6	12° 15′ 28 40° 39′ 06.5	12° 15′ 24.4 40° 39′ 06.5	12° 15′ 23.1 40° 39′ 07.8	
SiO_2	48.49	48.34	48.38	48.18	48.09	48.65	48.53	0.048
TiO_2	3.21	3.20	3.20	2.98	3.00	3.03	3.03	0.006
Al_2O_3	13.83	13.63	13.69	14.15	14.12	14.12	14.04	0.031
Fe_2O_3	16.08	16.11	16.07	15.43	15.41	15.48	15.47	0.005
MnO	0.246	0.246	0.244	0.236	0.236	0.237	0.238	0.001
MgO	5.43	5.42	5.30	5.39	5.30	5.46	5.39	0.051
CaO	9.57	9.51	9.57	9.89	9.88	9.79	9.83	0.012
Na_2O	3.01	3.04	3.03	3.05	3.03	2.97	2.99	0.014
K_2O	0.718	0.754	0.726	0.682	0.688	0.671	0.673	0.004
P_2O_5	0.518	0.505	0.514	0.474	0.477	0.483	0.483	0.003
SO_3	0.047	0.096	0.057	0.012	0.011	0.041	0.044	0.002
Ni (ppm)[c]	14.7 (0.004)	15 (0.665)	13.4 (0.674)	16.6 (0.004)	15.6 (0.66)	17.5 (0.004)	16.1 (0.004)	
LOI	−0.77	−1.09	−0.82	−0.37	−0.42	−0.57	−0.64	
Total	100.37	99.76	99.95	100.10	99.83	100.36	100.07	
Quartz	0	0	0	0	0	0	0	
Plagioclase	47.74	47.38	47.59	49.16	49.12	48.62	48.53	
Orthoclase	4.25	4.49	4.31	4.08	4.14	3.96	4.02	
Nepheline	0	0	0	0.00	0	0	0.00	
Diopside	18.4	18.97	18.93	19.42	19.47	18.59	19.06	
Hypersthene	13.51	12.3	13.16	9.85	10.11	13.99	13.20	
Wollastonite	0	0	0	0.00	0	0	0.00	
Olivine	6.44	7.23	6.34	8.40	8.03	5.68	6.00	
Ilmenite	6.12	6.12	6.12	5.72	5.77	5.79	5.79	
Magnetite	2.33	2.35	2.35	2.26	2.26	2.26	2.26	
Apatite	1.2	1.18	1.2	1.11	1.11	1.14	1.14	
Mg#[d]	42.6	42.6	42.1	43.50	43.1	43.7	43.40	

All data determined using a PANalytical Axios Advanced XRF spectrometer at the University of Leicester, UK. Samples prepared using standard XRF preparation techniques. Numbers in parentheses denote analytical errors (1 std).
[a] Porphyritic hypocrystalline samples from main flow unit.
[b] Glassy scoria deposit from above fissure.
[c] Analytical error (1σ) for Ni in parentheses.
[d] MgO/(MgO/FeO) (assuming 90% Fe as Fe^{2+}).

Manda Hararo graben (Barrat et al., 2003), these are transitional from sub-alkaline to alkaline. Plots of MgO vs. Ni and MgO vs. TiO_2 comparing the newly erupted basalts to the analyses reported by Barberi et al (1975) and Barrat et al. (2003) are shown in Fig. 4. The new samples lie towards the differentiated end of the regional trend, with Mg-numbers of 42–43, and low Ni contents. There is essentially no difference in bulk composition between the August 2007 lavas (Mg#'s 42.1–42.6) and the June 2009 lavas (Mg#'s 43.1–43.7).

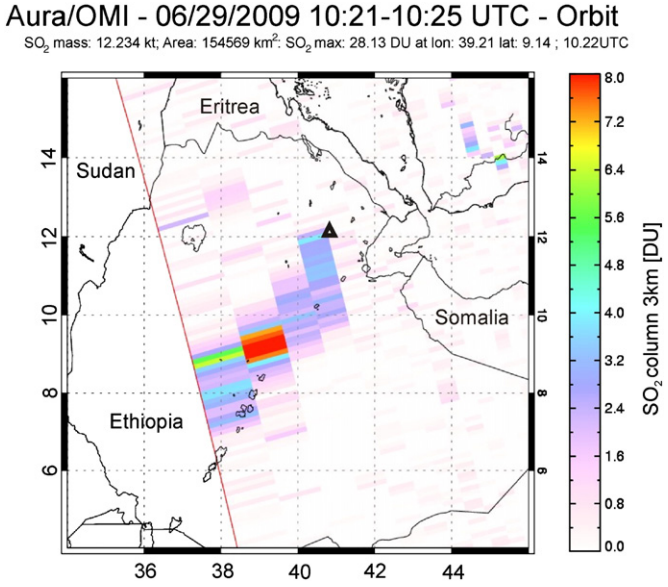

Fig. 3. SO_2 column amounts (in Dobson Units [DU]; 1 DU = 28.5 mg m^{-2}) retrieved from OMI measurements at ~10:23 UTC on 29 June (colour-coded pixels) superimposed on a map showing national boundaries. Location of eruptive vent is illustrated by the triangle. A concentrated region of SO_2 can be seen within the plume around 384 km downwind.

5. Partitioning of magma between intrusion and eruption

5.1. Dyke and lava volumes for 2007 and 2009 eruptions

The relations between intrusive and extrusive melt volumes in active magmatic systems, whether for the entire system (i.e. White et al., 2006 and references therein) or between magma supplied periodically to the shallow crust from a deeper source (i.e. between lava flows and dykes), are typically hard to constrain with any degree of confidence. With respect to the latter of theses, observations from the Krafla rifting suggest that during the 9 yr event a marked change occurred, whereby initially high intrusive to extrusive ratios (I:E) where lowered by an increasing volcanic output towards the end of the cycle (Harris et al., 2000). In the case of the recent Afar dyking events the high-resolution geophysical data available (i.e. Ebinger et al., 2008; Keir et al., 2009; Hamling et al., 2009) have allowed the volumes of successive intrusions to be modelled with unusually high precision (Table 3). Using elastic dislocation models, based on InSAR and GPS data, Hamling et al. (2009) established the locations and opening profiles of seven dykes intruded along the DMH rift between June 2006 and November 2007, and derived volume estimates for each intrusion. These extend to a depth of ~10 km, coincident with a magmatic source region identified from high-resolution seismic

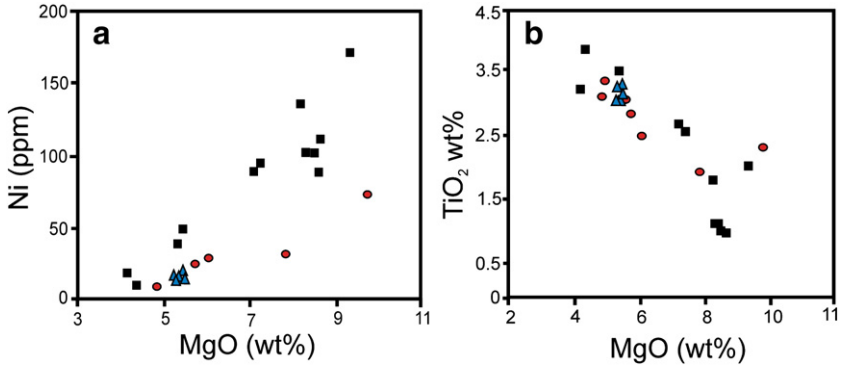

Fig. 4. Geochemical plots of (a) MgO vs. Ni and (b) MgO vs. TiO_2 comparing the recently erupted basaltic lavas (triangles) with other reported (whole rock) analyses for basalts from the around the Dabbahu volcano (circles) and ~60 km south of eruption site along the Manda Hararo graben (squares). The 2007 and 2009 samples are less primitive than many of the other basalts. Data for recent eruptions shown in Table 2. Dabbahu data from Barberi et al. (1975); Manda Hararo data from Barrat et al. (2003).

measurements (Keir et al., 2009), and therefore likely approximate the volume of the entire intrusion. Parameters from the August 2007 modelled intrusion suggest a dyke of volume of $48 \pm 1 \times 10^6$ m^3, oriented 334° and 9.1 km in length, causing surface opening of ≤1.6 m (Hamling et al., 2009). The region of maximum extension along the intrusion track is coincident with the eruptive fissure. Applying the same inversion method to InSAR data from the June 2009 intrusion reveals a similar scenario; a dyke with maximum surface opening of ≤1.5 m and a volume of $50 \pm 7 \times 10^6$ m^3 of magma. Both eruptive fissures opened along the southern sections of their feeder dykes, at the furthest lateral extent from the source region (Fig. 5).

Volumes of all the intrusive and eruptive events during the current Afar phase are listed in Table 3 and the temporal trend of intrusive and extrusive magma volumes shown in Fig. 6b. The individual volume ratios between intrusive and extrusive emplacement for the August 2007 and June 2009 events are approximately 10:1 and 5:1, respectively. As a 2 m wide dyke will have cooled to around half its initial temperature within 12 days (Fowler, 1990) (return time of recent dykes in Afar in 1–6 months) it is unlikely that the recent eruptions have involved significant amounts of previously intruded material.

5.2. Cumulative volume ratios during a rifting episode

The best studied rifting period in an analogous setting prior to the current Afar activity was the 1975–1984 Krafla rifting cycle in Iceland (e.g. Bjornsson et al., 1979; Tryggvason, 1984; Einarsson, 1991). During 9 yr of activity at Krafla 20 individual dykes were intruded along the rift, accompanied by nine basaltic eruptions. Estimates of intruded volumes are available from geodetic models of inflation and deflation of the inferred magma source by Ewart et al. (1991). The volume of erupted material can also be estimated via field and remote sensing observations (Bjornsson et al., 1977, 1979; Harris et al., 2000 and references therein). The temporal pattern of magma partitioning between intrusive and extrusive activity during the Krafla cycle (shown in Fig. 6) demonstrates a distinct change between from a dominantly intrusive to a dominantly extrusive regime after ~4 yr of activity (Harris et al., 2000). During the initial and chiefly intrusive phase the volume ratio of cumulative intrusive to extrusive melt varied from 444:1 and 148:1. By the fifth basaltic eruption, in 1980 (coincident with the ~15th dyke intrusion), the majority of melt supplied from the central magma source was being erupted rather than intruded. Numerical modelling of the Krafla activity by Buck et al. (2006) attributed the increasing volcanic output to a continual relaxation of along-axis stresses by successive dyke injections, allowing for greater vertical (vs. horizontal) propagation during later intrusion events. The final intrusive and extrusive magma ratio for the entire 9 yr episode was ~3:1 (Harris et al., 2000). Long-term intrusive–extrusive melt ratios for the (slow spreading) Mid Atlantic Ridge and the (fast spreading) East Pacific Rise have been estimated, based on structural studies, to be between 5–10:1 and 5–8:1 respectively (White et al., 2006). These estimates are currently too imprecise to resolve any differences resulting from variations in spreading rate. It is still unclear how typical the episodic rifting style seen in Iceland and Afar is to oceanic systems.

The current rifting phase in the DMH has produced thirteen dykes with a cumulative volume of $2758 \pm 227 \times 10^6$ m^3 (2.758 km^3) and two basaltic eruptions with a total volume of $15.6 \pm 3.1 \times 10^6$ m^3 (Fig. 6b), giving a cumulative intrusive–extrusive balance of ~180:1 at the time of writing (October 2009). The current pattern of the cumulative intrusive–extrusive volume ratio for Afar is shown alongside the corresponding data for Krafla in Fig. 6. Both phases began as predominantly intrusive events, with very high intrusive volumes relative to the volcanic output (ratios of 100's:1). At Krafla this was subsequently "balanced", to obtain a final ratio of 3:1, by a period of dominantly eruptive activity.

Table 3
Intrusive and extrusive volumes for dyking/eruptive events since September 2005.

	Sept 2005	June 2006	July 2006	Sept 2006	Dec 2006	Jan 2007	Aug 2007	Nov 2007	April 2008	July 2008	Oct 2008	Feb 2009	June 2009	Total ($\times 10^6$ m^3)
Intruded volume ($\times 10^6$ m^3)	1750 ± 250[a]	120 ± 10[b]	47 ± 17[b]	88 ± 14[b]	58 ± 11[b]	37 ± 13[b]	48 ± 1[b]	150 ± 10[b]	90 ± 20[c]	70 ± 20[c]	170 ± 1[c]	80 ± 3[c]	50 ± 7[c]	2758 ± 227
Erupted volume ($\times 10^6$ m^3)							4.6 ± 1.5[d]						11 ± 1.8[d]	15.6 ± 3.3[d]

[a] Grandin et al., 2009.
[b] Hamling et al., 2009.
[c] I. Hamling unpublished data.
[d] Estimate from field and remote sensing observations.

Please cite this article as: Ferguson, D.J., et al., Recent rift-related volcanism in Afar, Ethiopia, Earth Planet. Sci. Lett. (2010), doi:10.1016/j.epsl.2010.02.010

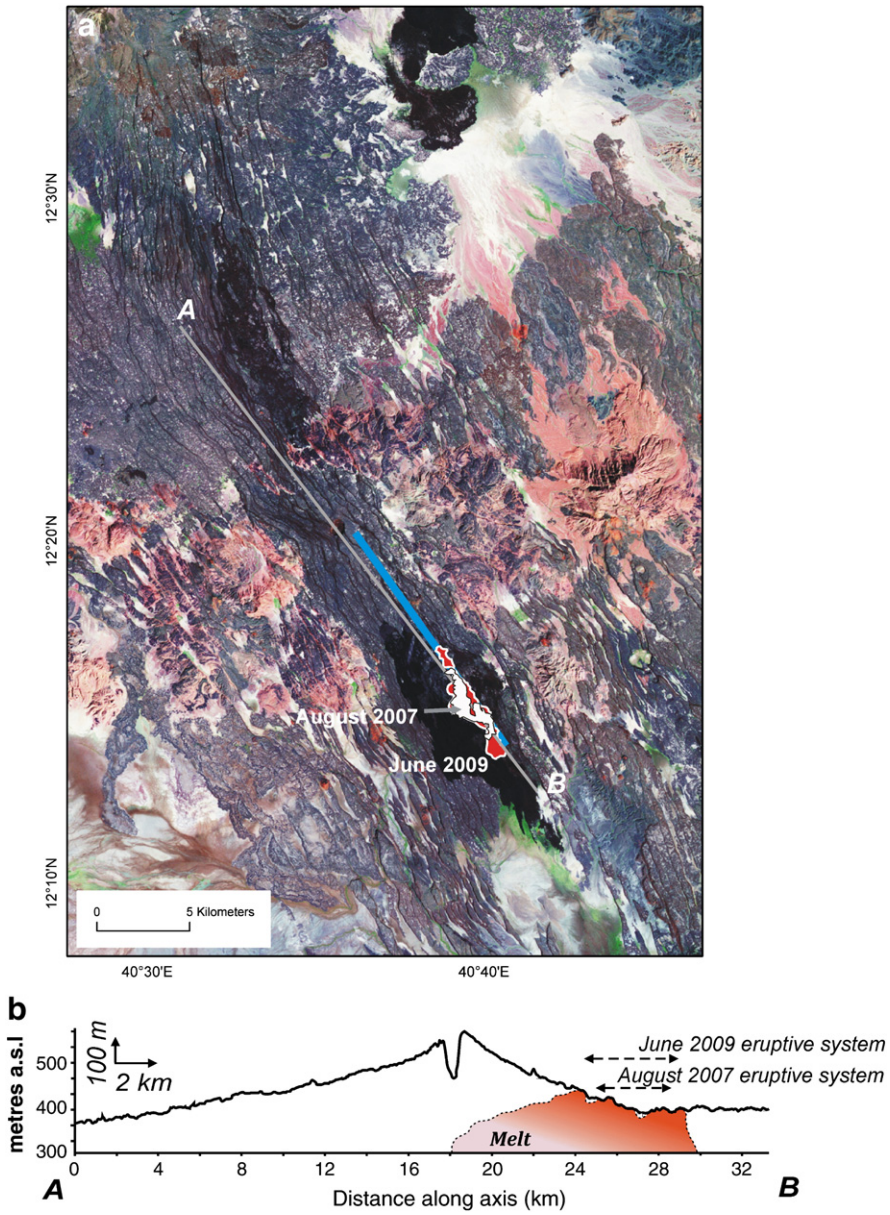

Fig. 5. (a) False colour Landsat ETM+ (Enhanced Thematic Mapper) image of the central part of the Dabbahu–Manda Hararo rift (regional location shown in Fig. 1b). Basaltic rocks generally appear dark whilst the more siliceous lava flows that flank the rift centre appear red. Vegetation is green. Blue line is the modelled track of the August 2007 dyke (by Hamling et al., 2009). Both the 2007 (white outline) and 2009 (red outline) basaltic eruptions occurred along the southern part of the intrusion. The most recent basaltic volcanism prior to 2007 (identified as the most un-deformed basaltic flows) can be seen on the northern and southern margins of the central axial topography (b) cross section showing topographic profile along the rift axis, locations of the recent eruptive fissures and schematic illustration of the feeder dyke. In the central part of the rift zone the axial graben is replaced by a region of enhanced volcanic topography, coincident with a seismically imaged subsurface region of magma storage (identified by Keir et al., 2009). (For interpretation of the references to colour in this figure legend, the reader is referred to the web version of this article.)

6. Surface characteristics of volcanism

We compare observations of first-order physical volcanic parameters for the Afar and Krafla rifting events. Fig. 7 shows the evolution of eruptive parameters for Krafla and also the August 2007 and June 2009 Afar events. At Krafla, all observed physical features (fissure length, duration, areal extent and volume) increased in magnitude throughout the 9 yr period and the size of an individual eruption was partly influenced by its position in the sequence. The recent eruptions in Afar have been of a comparable size to those at Krafla at a similar stage since the start of the cycle. Some studies (e.g. Perfit and Chadwick, 1998; Sinton et al, 2002) have suggested that such physical characteristics can have a proportional relationship to the spreading rate. If such relations do exist, observational data on volcanism could provide important, and accessible, constraints on subsurface processes However, an important factor influencing the long-term style of volcanism at a rift system is whether (eruptible) melt is present below the rift axis. A permanent sub-axial magma chamber is generally considered only to be a feature of faster spreading systems ($\sim >50$ mm yr^{-1}; Sinton and Detrick, 1992; Phipps-Morgan and Chen, 1993), although long lived melt bodies may also exist along sections of slower spreading system (Singh et al., 2006). The contrast between intermittent or permanent availability of magma is likely to exert a fundamental control on whether volcanism is episodic or steady state, and would therefore be expected to influence the characteristic sizes and timings of a sequence of eruptions. The current catalogue of volcanic data for oceanic (and terrestrial) rifts, although growing is still too limited to draw any clear conclusions on this. In the case of slower spreading systems where episodic rifting occurs, the

Please cite this article as: Ferguson, D.J., et al., Recent rift-related volcanism in Afar, Ethiopia, Earth Planet. Sci. Lett. (2010), doi:10.1016/j.epsl.2010.02.010

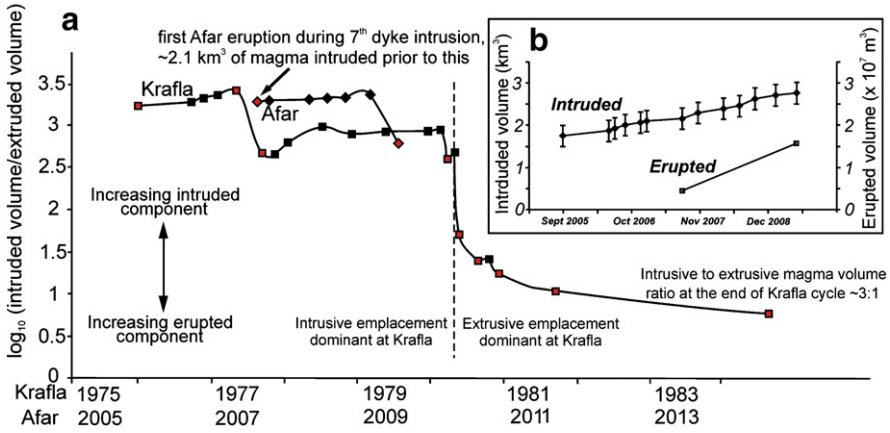

Fig. 6. (a) Temporal trend of cumulative intrusive to extrusive magma volume ratios during the Krafla rifting cycle and from the currently (post 2005) ongoing activity in Afar. Magma supplied to the Krafla system during the initial part of the rifting phase was dominantly emplaced via intrusive processes. The bulk of the volcanic flux occurred during the latter stage of the cycle where almost all supplied melt was erupted. The recent Afar activity has a similar regime for the corresponding stage of the Krafla cycle. Both extrusive volumes have been corrected for a porosity of 30%. Red symbols indicate dyking events that included eruptions. Intrusive volumes at Krafla from Ewart et al, 1991. Erupted volumes from Bjornsson et al., 1977, 1979 and Harris et al, 2000 and references therein. (b) Current trends for intruded and erupted magma volume in the DMH rift. Note that the erupted scale is ×100 the intruded. (For interpretation of the references to colour in this figure legend, the reader is referred to the web version of this article.)

recognition that such a pattern of increasing eruption sizes may exist could provide a new context in which to interpret intermittent oceanic observations (see discussion in Section 8.2). In order to derive meaningful correlations between eruptive parameters and spreading rates (e.g. Sinton et al., 2002), the physical features relating to a single eruption/eruptive period must be accurately resolved. In case of an episodic rifting style, focussing the volcanic component to the latter stages of a rifting phase increases the likelihood that newly emplaced flows and eruptive systems will be rapidly resurfaced, limiting the time available for detection. Even on the subaerial rift systems in Iceland and Afar, the subsequent identification of a single eruptive unit would be problematic without contemporaneous observations.

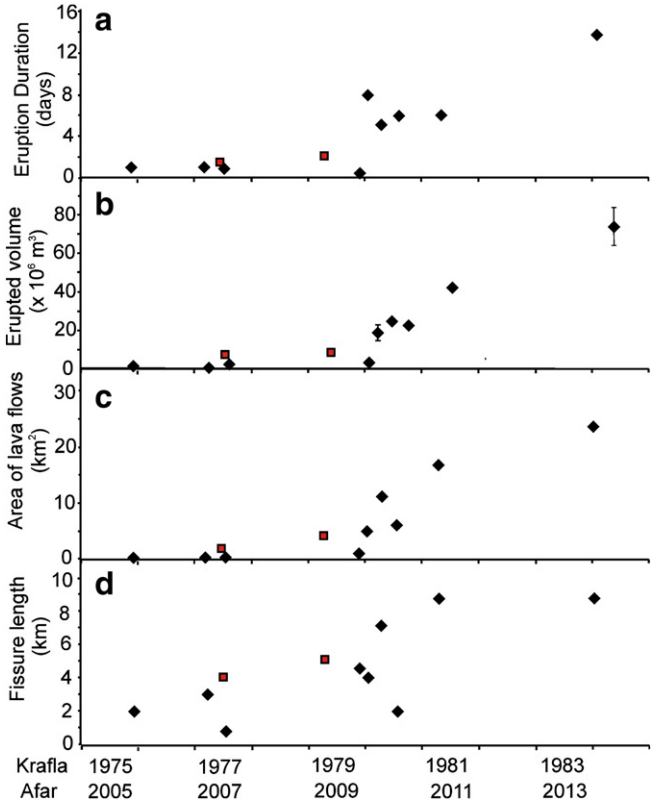

Fig. 7. Temporal patterns of first-order physical parameters for basaltic eruptions from the Afar (squares) and Krafla (diamonds) rifting phases. (a) Eruption duration, (b) erupted volume (DRE corrected for 30% porosity), (c) area of eruption products, (d) fissure length. Trend lines are for Krafla data only. All observed parameters show an overall increase during the Krafla cycle as individual eruptions became larger in magnitude. See Section 6 for discussion.

7. Volcanic topography and eruption locations

7.1. Relations between dyking and rift morphology

Structural analysis of recent (post September 2005) and existing fault structures along the DMH segment have identified the majority of brittle surface deformation to be magmatic (i.e. dyke induced) in origin (Rowland et al., 2007). Recent seismic studies (Keir et al., 2009) have argued for a zone of magma accretion beneath the central section of the rift, corresponding with a region of axial volcanic topography, the Ado' Ale Volcanic Complex (AVC) (Figs. 1b and 5a), as a key factor in maintaining the segmentation of the rift zone along the Red Sea system. The coincidence of a central zone of magma accretion with the axial topography (Fig. 5b) agrees with predictions made by numerical modelling of successive intrusive events from a centralised magma source by Buck et al. (2006). Buck et al. argue that eruptions will most likely be associated with dykes with shorter lengths, thereby creating topography around the central magma source. In this model the stress effects of significant axial relief act to focus future eruptions at the margins of the central topography. Conversely, dismantling by normal faulting makes eruptions more likely at greater distances along the axis. Both the eruptions in Afar have been fed by dykes ~9 km long. This length is typical of many of the recent dykes (8–9 km), but much shorter than the initial September 2005 intrusion (~60 km) and also intrusions in July 2006 (~10 km) and November 2007 (~11 km) (Hamling et al., 2009).

7.2. Locations of basaltic fissure eruptions in the DMH rift

Imagery from the spaceborne Landsat ETM+ instrument (Fig. 5a) shows that the regions of most recent basaltic volcanism (i.e. those areas that are least faulted) correspond to the slopes/margins of the central edifice. One consequence of the apparent focussing of volcanic activity in these regions is the resulting difficulty in identifying previous eruptions, the products of which are continually resurfaced. For example, if there had been no observations of the August 2007 event at the time, it is likely the products would subsequently have been attributed to the later 2009 event. The use of thermal data acquired during, or shortly after, eruption has proved to be

Please cite this article as: Ferguson, D.J., et al., Recent rift-related volcanism in Afar, Ethiopia, Earth Planet. Sci. Lett. (2010), doi:10.1016/j.epsl.2010.02.010

remarkably useful in identifying the products of the most recent event (Figs. 1e and 2b, c). If the characteristics of volcanic systems fed from a central magma source are to be used to constrain the subsurface and rifting processes, then it is desirable to reconstruct accurately the volume and extent of previous individual eruptions.

8. Discussion

8.1. Size and frequency of eruptions during a rifting episode

The basaltic eruptions observed thus far during the rifting phase in August 2007 and June 2009 show many similarities to those that occurred during the comparable stage (i.e. within 5 yr of initiation) of the Krafla cycle. Magma partitioning at Krafla operated under two distinct regimes, with the bulk of each batch of melt supplied from the central chamber being intruded with or without accompanying eruptions. Overall, the 9 yr cumulative volcanic flux accounted for ~25% of the total magma supply (Harris et al., 2000). As magma transport to the shallow part of the rift zone is not continuous (i.e. during discrete dyke injections) then any marked increase in the trend of the cumulative erupted volume must be accommodated by either larger single eruptions or through a greater number of dyking intrusions that feed small to medium-sized eruptions. The temporal pattern of intrusive to extrusive magma volumes and of physical eruptive parameters activity observed at Krafla (Figs. 6 and 7) (Harris et al., 2000) clearly shows that in this system the former was the case. Numerical models based on the Krafla dykes (Buck et al., 2006) show that once stresses along a rift zone have been sufficiently relieved, via repeated dyke injections, the ability of successive intrusions to propagate upwards rather than laterally is increased and hence extrusion becomes more likely.

8.2. Long-term volcanic fluxes and spreading rates

Extension across the Red Sea system in Afar is currently ~16 mm yr^{-1} (Vigny et al., 2006). Rifting since 2005 has presently caused ~5–8 m of extension across the DMH rift zone (Hamling et al., 2009) and has been accompanied by a bulk volcanic flux of $\sim 15.6 \times 10^6$ m^3. Using the long-term spreading rate, this gives a low volcanic output of $\sim 0.003–0.005 \times 10^6$ m^3 yr^{-1}. The same calculation made for the Krafla episode, (9 m of extension accompanied by a bulk lava volume of $\sim 281 \times 10^6$ m^3 of lava and a long-term extension rate of 20 mm yr^{-1}) gives a significantly larger time-averaged flux of 0.4×10^6 m^3 yr^{-1}. Although this neglects any differences in geodynamic setting (i.e. the Icelandic hotspot), comparing the pattern of intrusive to eruptive behaviour at Krafla with the large number of purely intrusive events thus far in the Afar phase leads us to conclude that the above value for time-averaged flux in the DMH rift is a significant underestimate. Furthermore, the numerous basaltic flows that can be seen on the surface of the DMH rift (e.g. in Fig. 5) also suggest that an averaged volcanic flux of $<0.005 \times 10^6$ m^3 yr^{-1} is unlikely to be representative of this system.

8.3. Forecast for future basaltic eruptions in Afar

Pursuing the dyking model of Buck et al. (2006) with respect to DMH rift system suggests that once a critical threshold of extension is attained along the DMH rift, the dominant emplacement style for most the magma supplied to the rift will be by eruption rather than endogenous growth from intrusion. Our estimates of the partitioning of magma volume between intrusive dykes and extrusive lava flows, which is consistent thus far with the corresponding period of the Krafla rifting cycle, has intriguing implications for assessing both the volumes of subsurface melts, and relating intermittent volcanic observations to a sustained period of active rifting. The temporal trend of eruption sizes at Krafla (Fig. 7) suggests that, at least in the case of episodic rifting, the magnitude of any one volcanic event may depend on the most recent preceding activity, and that eruptions of varying sizes are not randomly distributed through time. If, over the course of a rifting cycle, the size of an eruption depends on the stage in the rifting cycle at which it occurs, then data on previous eruptive and intrusive events could provide a means of forecasting likely future volcanism. This reasoning provides the basis for a forward model to predict the likelihood and size of future eruptions in the DMH rift. We expect therefore that, should the current magma supply in the DMH rift be maintained, the volcanic flux will increase significantly from its current level and will be accommodated by eruptions of increasingly larger magnitude (i.e. of greater volume, duration and spatial extent). These are likely to be located in the central rift, within 10–15 km of the rift centre, on either the northern or southern margins of the central Ado' Ale volcanic complex (Fig. 3) As the two eruptions documented here are of relatively small magnitude, and as the major magmatic activity in Afar continues to be intrusive in nature, we forecast that the DMH rift system currently has a high potential to produce small–medium volume (i.e. $10–30 \times 10^6$ m^3) basaltic eruptions and a longer term potential (next 5–10 yr) of larger magnitude events (i.e. an erupted volume of $>50 \times 10^6$ m^3).

9. Conclusions

Opportunities to observe an active rifting cycle are extremely rare. The ongoing Afar phase is the first to be observed on land since the 1975–1984 Krafla cycle and the first in the age of high-resolution multispectral satellite observations. By integrating analysis of satellite imagery, field observations and available geodetic data we have been able to record and characterise the two basaltic eruptions that have occurred thus far during the Afar rifting cycle. Both eruptions were short-lived events that had volumes, durations, fissure lengths and mean effusion rates similar to basaltic fissure eruptions that occurred during the early stages of the Krafla phase. The SO_2 emissions observed by OMI during each event are consistent with volatile loss from the respective erupted volumes. Combining these physical observations with geodetic inversions of the intrusive activity in Afar allows the current cumulative mass balance between intrusive and extrusive magmatism for the rifting phase thus far to be constrained at ~180:1. Although the activity since 2005 has been primarily intrusive in nature, observations of the Krafla cycle (i.e. Bjornsson et al., 1979; Tryggvason, 1984) and models of repeated dyke emplacement (Buck et al., 2006) suggest that, should magma supply be maintained, a volumetrically significant volcanic phase may occur as the Afar activity progresses. The implication of this analysis is that future eruptions in the DMH (over the next ~10 yr) have the potential to be of greater magnitude than the currently observed events. It is likely that future eruptive fissures will be >5 km in length and located around the topographic margins of the central Ado' Ale volcanic complex.

Through continued observations of future eruptions we hope to build on the ideas presented here regarding the temporal, spatial and volumetric relationships between intrusive and extrusive magmatism in the DMH system. Future integration of volcanological observations with data from the ongoing geophysical (i.e. Wright et al., 2006; Ebinger et al., 2008; Hamling et al., 2009; Keir et al., 2009; Grandin et al., 2009) and geochemical studies in Afar should provide a valuable (and rare) opportunity to constrain the links between the volcanic, plutonic and tectonic features of an active rift system, this will hopefully help inform studies on other (i.e. oceanic) systems.

Acknowledgments

This work was carried out as a part of the NERC-funded Afar consortium (NE/E006469/1, NE/E005535/1). We acknowledge the general, and generous, support of many Ethiopian, UK and other

Please cite this article as: Ferguson, D.J., et al., Recent rift-related volcanism in Afar, Ethiopia, Earth Planet. Sci. Lett. (2010), doi:10.1016/j.epsl.2010.02.010

colleagues within this consortium. We would also like to thank the Ethiopian Air Force for generously providing helicopter support during both the eruptions. We are very grateful to S.A Soule and one anonymous reviewer for providing detailed and thought provoking comments that significantly improved the original manuscript.

References

Ayele, A., Jacques, E., Kassim, M., Kidane, T., Omar, A., Tait, S., Nercessian, A., de Chabalier, J.B., King, G., 2007. The volcano-seismic crisis in Afar, Ethiopia, starting September 2005. Earth Planet. Sci. Lett. 255, 177–187.

Barberi, F., Tazieff, H., Varet, J., 1972. Volcanism in the Afar depression: its tectonic and magmatic significance. Tectonophysics 15, 19–29.

Barberi, F., Ferrara, G., Santacroce, R., Treuil, M., Varet, J., 1975. A transitional basalt–pantellerite sequence of fractional crystallisation, the Boina Centre (Afar Rift, Ethiopia). J. Petrol. 16, 22–56.

Barrat, J.A., Joron, J.L., Taylor, R.N., Fourcade, S., Nesbitt, R.W., Jahn, B.M., 2003. Geochemistry of basalts from manda Hararo, Ethiopia: LREE-depleted basalts in Central Afar. Lithos 69, 1–13.

Bjornsson, A., Saemundsson, K., Einarsson, P., Tryggvason, E., Gronvald, K., 1977. Current rifting episode in North Iceland. Nature 266, 318–323.

Bjornsson, A., Johnsen, G., Sigurdsson, S., Thorbergsson, G., Tryggvason, E., 1979. Rifting of a plate boundary in North Iceland 1975–1978. J. Geophys. Res. 84, 3029–3038.

Buck, W.R., Einarsson, P., Brandsdottir, B., 2006. Tectonic stress and magma chamber size as controls on dike propagation: constraints from the 1975–1984 Krafla rifting episode. J. Geophys. Res. 111, B12404.

Chadwick, W.W., Embley, R.W., Fox, C.G., 1995. SeaBeam depth changes associated with recent lava flows, CoAxial segment, Juan de Fuca Ridge: evidence for multiple eruptions between 1981 and 1993. Geophys. Res. Lett. 22, 167–170.

Clocchiatti, R., Métrich, N., Weiss, J., 1980. Petrologie et mineralogie des basaltes d'Asal, Afar: Bulletin CNRS-PIRPSEV (Centre National de la Recherche Scientifique, Prévision et Surveillance des Eruptions Volcaniques), no. 10, 18 p.

Crisp, J.A., 1984. Rates of magma emplacement and volcanic output. J. Volcanol. Geotherm. Res. 20, 177–211.

Draxler, R.R., Rolph, G.D., 2003. HYSPLIT (HYbrid Single-Particle Lagrangian Integrated Trajectory) Model access via NOAA ARL READY Website (http://www.arl.noaa.gov/ready/hysplit4.html). NOAA Air Resources Laboratory, Silver Spring, MD.

Ebinger, C., Keir, D., Ayele, A., Calais, E., Wright, T., Belachew, M., Hammond, J., Campbell, E., Buck, R., 2008. Capturing magma intrusion and faulting processes during continental rupture: seismicity of the Dabbahu Afar rift. Geophys. J. Int. 174, 1138–1152.

Einarsson, P., 1991. The Krafla rifting episode 1975–1989. In: Gardarsson, A., Einarsson, P. (Eds.), N´att´ura Myvatns, The Nature of Lake Myvatn. Icelandic Nature Science Society, Reykjavic, pp. 97–139.

Embley, R.W., Chadwick, W.W., Clague, D.A., Stakes, D., 1999. 1998 eruption of Axial Volcano: multibeam anomalies and sea-floor observations. Geophys. Res. Lett. 26, 3425–3428.

Embley, R.W., Chadwick, W.W., Perfit, M.R., Smith, M.C., Delaney, J.R., 2000. Recent eruptions on the CoAxial segment of the Juan de Fuca Ridge: implications for mid-ocean ridge accretion processes. J. Geophys. Res. 105, 16,501–16,526.

Ewart, J.A., Voight, B., Bjornsson, A., 1991. Elastic deformation models of Krafla Volcano, Iceland, for the decade 1975 through 1985. Bull. Volcanol. 53, 436–459.

Fowler, M.R.C., 1990. The Solid Earth: An Introduction to Global Geophysics. Cambridge University Press, Cambridge, p. 283.

Grandin, R., Socquet, A., Binet, R., Klinger, Y., Jacques, E., de Chabalier, J.B., King, G.C.P., Lasserre, C., Tait, S., Tapponier, P., Delorme, A., Pinzuti, P., 2009. September 2005 Manda Hararo–Dabbahu rifting event, Afar Ethiopia: constraints provided by geodetic data. J. Geophys. Res. 114, B08404.

Hamling, I.J., Ayele, A., Bennati, L., Calais, E., Ebinger, E.J., Keir, D., Lewi, E., Wright, T., Yirgu, G., 2009. Geodetic observations of the ongoing Dabbahu rifting episode: new dyke intrusions in 2006 and 2007. Geophys. J. Int. 178, 989–1003.

Harris, A.J.L., Murray, J.B., Aries, S.E., Davies, M.A., Flynn, L.P., Wooster, M.J., Wright, R., Rothery, D.A., 2000. Effusion rate trends at Etna and Krafla and their implications for eruptive mechanisms. J. Volcanol. Geother. Res. 102, 237–270.

Hayward, N.J., Ebinger, C.J., 1996. Variations in the along-axis segmentation of the Afar Rift System. Tectonics 15, 244–257.

Smithsonian Institution, 2007. Manda Hararo. Bull. Global Volcanism Network 32, 7.

Smithsonian Institution, 2009. Manda Hararo. Bull. Global Volcanism Network 34, 6.

Keir, D., Hamling, I., Ayele, A., Calais, E., Ebinger, C., Wright, T.J., Jacques, E., Mohammed, K., Hammond, J.O.S., Belachew, M., Baker, E., Rowland, J.V., Lewi, E., Bennati, L., 2009. Evidence for focused magmatic accretion at segment centers from lateral dike injections captured beneath the Red Sea rift in Afar. Geology 37, 59–62.

Lahitte, P., Gillot, P.Y., Courtillot, V., 2003. Silicic central volcanoes as precursors to rift propagation: the Afar case. Earth Planet. Sci. Lett. 207, 103–116.

Levelt, P.F., van den Oord, G.H.J., Dobber, M.R., Mälkki, A., Visser, H., de Vries, J., Stammes, P., Lundell, J.O.V., Saari, H., 2006. The Ozone Monitoring Instrument. IEEE Trans. Geosci. Remote Sensing 44, 1093–1101.

Oppenheimer, C., Francis, P., 1997. Remote sensing of heat, lava and fumerole emissions from Erta'Ale volcano, Ethiopia. Int. J. Remote Sensing 18, 1661–1692.

Perfit, M.R., Chadwick, W.W., 1998. Magmatism at mid-ocean ridges: constraints from volcanological and geochemical investigations. In: Buck, W.R., Delaney, P.T., Karson, J.A., Lagabrielle, Y. (Eds.), Faulting and Magmatism at Mid-Ocean Ridges. : Geophys. Monograph, 106. AGU, Washington, D.C., pp. 59–115.

Phipps Morgan, J., Chen, Y.J., 1993. Dependence of ridge-axis morphology on magma supply and spreading rate. Nature 364, 706–708.

Rowland, J.V., Baker, E., Ebinger, C.J., Keir, D., Kidane, T., Biggs, J., Hayward, N., Wright, T.J., 2007. Fault growth at a nascent slow-spreading ridge: 2005 Dabbahu rifting episode, Afar. Geophys. J. Int. 171, 1226–1246.

Shaw, H.R., Jackson, E.D., Bargar, K.E., 1980. Volcanic periodicity along the Hawaiian–Emperor chain. Am. J. Sci. 280A, 667–708.

Singh, S.C., Crawford, W.C., Carton, H., Seher, T., Combier, V., Cannat, M., Canales, J.P., Dusunur, D., Escartin, J., Miranda, M., 2006. Discovery of a magma chamber and faults beneath a Mid-Atlantic Ridge hydrothermal field. Nature 442, 1029–1032.

Sinton, J.M., Detrick, R.S., 1992. Mid-ocean ridge magma chambers. J. Geophys. Res. 97 (B1), 197–216.

Sinton, J., Bergmanis, E., Rubin, K., Batiza, R., Gregg, T.K.P., Gronvold, K., Macdonald, K.C., White, S.M., 2002. Volcanic eruptions on mid-ocean ridges: new evidence from the superfast spreading East Pacific Rise, 17–19 S. J. Geophys. Res. 107, B2115.

Soule, S.A., Fornari, D.J., Perfit, M.R., Rubin, K.H., 2007. New insights into mid-ocean ridge volcanic processes from the 2005–2006 eruption of the East Pacific Rise, 9° 46′N 9° 56′N. Geology 35, 1079–1082.

Spampinato, L., Calvari, S., Oppenheimer, C., Lodato, L., 2008. Shallow magma transport for the 2002–3 Mt. Etna eruption inferred from thermal infrared surveys. J. Volcanol. Geoth. Res. 177, 301–312.

Tryggvason, E., 1984. Widening of the Krafla fissure swarm during the 1975–1981 volcano-tectonic episode. Bull. Volcanol. 471, 47–69.

Vigny, C., Huchon, P., Ruegg, J.C., Khanbari, K., Asfaw, L.M., 2006. Confirmation of Arabia slow motion by new GPS data in Yemen. J. Geophys. Res. 111, B02402.

Wadge, G., 1980. Output rate of magma from active central volcanoes. Nature 228, 253–255.

White, S.M., Crisp, J.A., Spera, F.J., 2006. Long-term volumetric eruption rates and magma budgets. Geochem. Geophys. Geosyst. 7, Q03010.

Wright, R., Flynn, L.P., Garbeil, H., Harris, A.J.L., Pilger, E., 2004. MODVOLC: near-real-time thermal monitoring of global volcanism. J. Volcanol. Geother. Res. 135, 29–49.

Wright, T.J., Ebinger, C., Biggs, J., Ayele, A., Yirgu, G., Keir, D., Stork, A., 2006. Magma-maintained rift segmentation at continental rupture in the 2005 Afar dyking episode. Nature 442, 291–294.

Yang, K., Krotkov, N.A., Krueger, A.J., Carn, S.A., Bhartia, P.K., Levelt, P.F., 2007. Retrieval of large volcanic SO_2 columns from the Aura Ozone Monitoring Instrument: comparison and limitations. J. Geophys. Res. 112, D24S43.

Yirgu, G., Ayele, A., Ayalew, D., 2006. Recent seismovolcanic crisis in Northern Afar, Ethiopia. Eos, Trans. AGU 87, 325–326.

Please cite this article as: Ferguson, D.J., et al., Recent rift-related volcanism in Afar, Ethiopia, Earth Planet. Sci. Lett. (2010), doi:10.1016/j.epsl.2010.02.010